Cell Reports

Shp-2 Is Dispensable for Establishing T Cell Exhaustion and for PD-1 Signaling *In Vivo*

Graphical Abstract

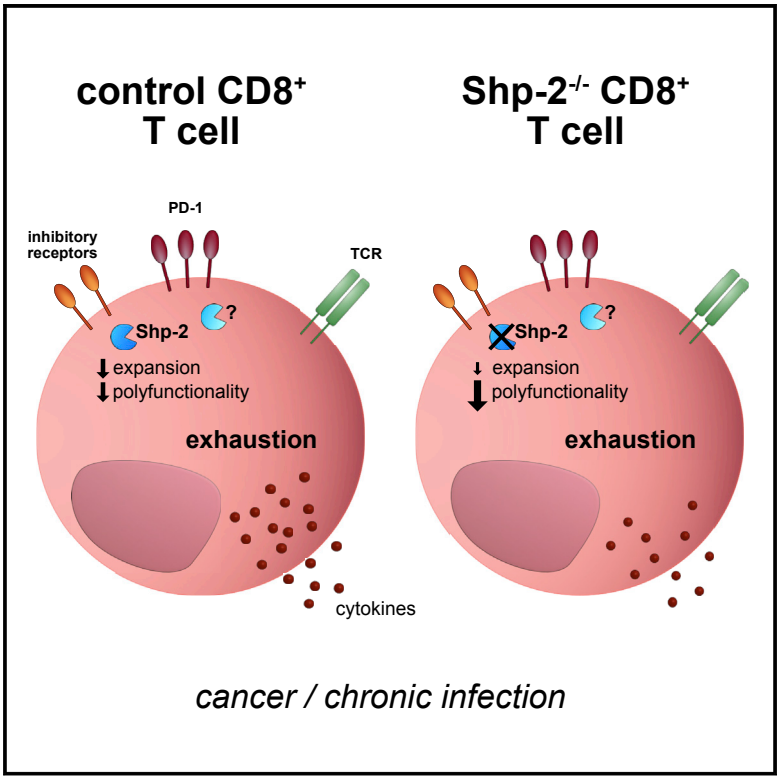

Authors

Giorgia Rota, Charlène Niogret, Anh Thu Dang, ..., Walter Birchmeier, Eric Vivier, Greta Guarda

Correspondence

greta.guarda@irb.usi.ch

In Brief

In vitro data indicate that Shp-2 is engaged by PD-1 and contributes to T cell exhaustion. Rota et al. show that Shp-2-deficient T cells acquire a dysfunctional state when exposed to chronic antigen *in vivo* and respond to PD-1 blockade, indicating the existence of additional signaling factors.

Highlights

- Shp-2 modulates selected T cell exhaustion features
- Shp-2 is not required for the global dysfunctional state of exhausted T cells
- Anticancer α-PD-1 treatment is beneficial in mice with Shp-2-deficient T cells

Rota et al., 2018, Cell Reports *23*, 39–49
April 3, 2018
https://doi.org/10.1016/j.celrep.2018.03.026

CellPress

Cell Reports
Report

Shp-2 Is Dispensable for Establishing T Cell Exhaustion and for PD-1 Signaling *In Vivo*

Giorgia Rota,[1] Charlène Niogret,[1] Anh Thu Dang,[1] Cristina Ramon Barros,[1] Nicolas Pierre Fonta,[1,7] Francesca Alfei,[2] Leonor Morgado,[1] Dietmar Zehn,[2] Walter Birchmeier,[3] Eric Vivier,[4,5,6] and Greta Guarda[1,7,8,*]

[1]Department of Biochemistry, University of Lausanne, 1066 Epalinges, Switzerland
[2]Division of Animal Physiology and Immunology, School of Life Sciences Weihenstephan, Technical University of Munich, 85354 Freising, Germany
[3]Cancer Research Program, Max Delbrueck Center for Molecular Medicine (MDC) in the Helmholtz Society, 13125 Berlin, Germany
[4]Centre d'Immunologie de Marseille-Luminy, Aix Marseille Université, Inserm, CNRS, 13288 Marseille, France
[5]Service d'Immunologie, Hôpital de la Timone, Assistance Publique-Hôpitaux de Marseille, 13005 Marseille, France
[6]Innate Pharma Research Labs, Innate Pharma, Marseille, France
[7]Institute for Research in Biomedicine, Università della Svizzera italiana, 6500 Bellinzona, Switzerland
[8]Lead Contact
*Correspondence: greta.guarda@irb.usi.ch
https://doi.org/10.1016/j.celrep.2018.03.026

SUMMARY

In chronic infection and cancer, T cells acquire a dysfunctional state characterized by the expression of inhibitory receptors. *In vitro* studies implicated the phosphatase Shp-2 downstream of these receptors, including PD-1. However, whether Shp-2 is responsible *in vivo* for such dysfunctional responses remains elusive. To address this, we generated T cell-specific Shp-2-deficient mice. These mice did not show differences in controlling chronic viral infections. In this context, Shp-2-deleted CD8$^+$ T lymphocytes expanded moderately better but were less polyfunctional than control cells. Mice with Shp-2-deficient T cells also showed no significant improvement in controlling immunogenic tumors and responded similarly to controls to α-PD-1 treatment. We therefore showed that Shp-2 is dispensable in T cells for globally establishing exhaustion and for PD-1 signaling *in vivo*. These results reveal the existence of redundant mechanisms downstream of inhibitory receptors and represent the foundation for defining these relevant molecular events.

INTRODUCTION

Chronic antigen exposure drives T cell exhaustion, a condition in which effector T cells progressively lose the capacity to produce multiple cytokines and proliferate (Pauken and Wherry, 2015). This phenomenon represents an adapted response reducing excessive T cell activation and collateral damage, but it also hampers immunity (Speiser et al., 2014). Exhausted T cells are characterized by the expression of inhibitory receptors, including programmed cell death 1 (PD-1). Blocking signaling by PD-1 and other inhibitory receptors restores T cell responses, effectively promoting disease control in cancer patients (Pauken and Wherry, 2015; Topalian et al., 2015). These findings reveal the potential of interfering with such inhibitory circuits and the need to understand the underlying molecular pathways.

Cytoplasmic tails of inhibitory receptors bear immunoreceptor tyrosine-based inhibition motifs (ITIMs) and immunoreceptor tyrosine-based switch motifs (ITSMs), which are phosphorylated upon engagement and act as docking sites for SH2 domain-containing protein tyrosine phosphatase (Shp)-2 (encoded by the *Ptpn11* gene) and the homologous Shp-1 (Siminovitch and Neel, 1998; Tajan et al., 2015). These phosphatases contain SH2 domains that interact with phosphotyrosines of receptors or signaling molecules, favoring accessibility of the catalytic site (Cunnick et al., 2001; Ekman et al., 2002; Noguchi et al., 1994; Siminovitch and Neel, 1998). Opposite to Shp-1, which dampens various signaling cascades, Shp-2 is mainly known for positively regulating growth factor or hormone receptor signaling, and its activity has been implicated in several malignancies (Chan et al., 2008; Prahallad et al., 2015; Tajan et al., 2015; Zhang et al., 2015).

Although several mouse models expressing a dominant-negative form of or lacking Shp-2 in T cells have been reported (Dong et al., 2015; Liu et al., 2017; Miah et al., 2017; Nguyen et al., 2006; Salmond et al., 2005; Zhang et al., 2013), a consensus on its role in these lymphocytes is missing. Some models showed defective T cell development and/or activation, whereas others exhibited normal T cells with unaltered or enhanced responses (Dong et al., 2015; Kwon et al., 2005; Liu et al., 2017; Miah et al., 2017; Nguyen et al., 2006; Salmond et al., 2005). In agreement with its known contribution to the mitogen-activated protein kinase (MAPK) pathway in cancerous cells and various tissues, multiple studies observed a positive role for Shp-2 in extracellular signal-regulated kinase (ERK) activation upon T cell receptor (TCR) triggering or interleukin (IL)-2 stimulation (Gadina et al., 1998; Kwon et al., 2005; Nguyen et al., 2006; Salmond et al., 2005).

In relation to T cell exhaustion, *in vitro* studies showed recruitment of Shp-2 to the cytoplasmic portion of PD-1 and other inhibitory receptors (Chemnitz et al., 2004; Hui et al., 2017; Latchman et al., 2001; Lee et al., 1998; Okazaki et al., 2001;

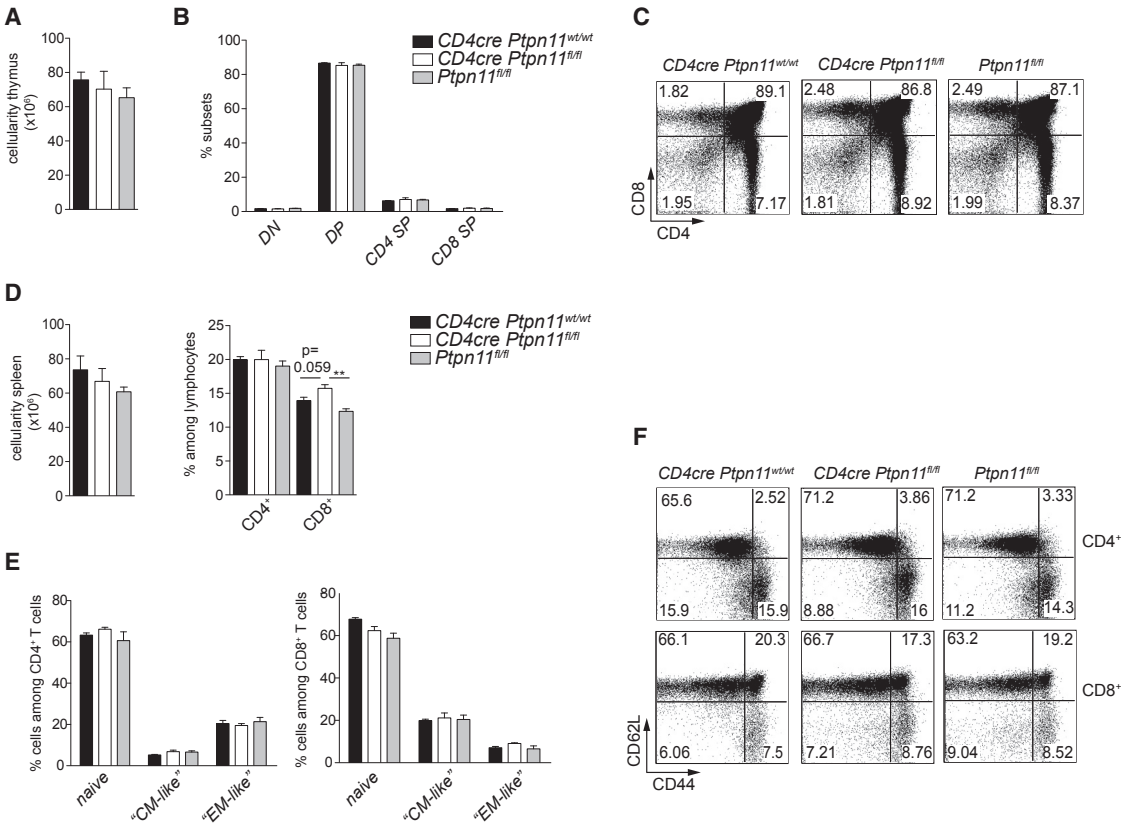

Figure 1. *CD4cre Ptpn11*$^{fl/fl}$ Mice Exhibit Normal T Cells

(A–C) Thymus cellularity (A) and percentage of double-negative (DN) thymocytes ($CD4^-CD8^-$), double-positive (DP) thymocytes ($CD4^+CD8^+$), and CD4 or CD8 single-positive (SP) thymocytes ($CD4^+CD8^-$ or $CD4^-CD8^+$, respectively) among lineage-negative lymphocytes (B) are depicted in *CD4cre Ptpn11*$^{wt/wt}$, *CD4cre Ptpn11*$^{fl/fl}$, and *Ptpn11*$^{fl/fl}$ mice. (C) Representative flow cytometry plots of CD4 and CD8 expression among lineage-negative thymocytes are illustrated. (A–C) Data are comparable in mice of 6 to 12 weeks.

(D) Spleen cellularity and percentages of $CD4^+$ ($CD4^+$ $CD3^+$) and $CD8^+$ ($CD8^+$ $CD3^+$) T cells (gated on lymphocytes) are illustrated.

(E and F) Percentages of naive ($CD44^{low\text{-}int}$ $CD62L^{high}$), CM-like ($CD44^{high}$ $CD62L^{high}$), and EM-like ($CD44^{high}$ $CD62L^{low}$) $CD4^+$ and $CD8^+$ T lymphocytes in the spleen (E) and a representative flow cytometry plot of CD62L and CD44 expression (F) are depicted.

Results represent mean ± SEM of n = 3–5 mice/group (A, B, D, and E) and are representative of at least two independent experiments (A–F). Only statistically significant differences are shown. $^{**}p \leq 0.01$; Student's t test. See also Figure S1.

Peled et al., 2018; Sheppard et al., 2004; Yamamoto et al., 2008; Yokosuka et al., 2012). Furthermore, a negative effect of Shp-2 on IL-2 production has been observed upon PD-1 engagement (Peled et al., 2018; Yokosuka et al., 2012). Shp-2 is therefore considered a central molecule for T cell exhaustion and one to target for therapeutic purposes. Yet work addressing its role in the context of chronic antigen exposure *in vivo* is missing. We therefore generated *CD4cre Ptpn11*$^{fl/fl}$ mice and tested the effect of Shp-2 ablation on T cell responses.

Following chronic viral infection, we found increased percentages of antiviral *Ptpn11*-deficient T cells compared to control mice. However, these cells exhibited compromised cytokine production and were unable to better control the infection. In addition, we subcutaneously engrafted mice with an immunogenic cancer. Tumor growth in *CD4cre Ptpn11*$^{fl/fl}$ mice was comparable to what was observed in controls, and these mice responded to α-PD-1 treatment. Therefore, Shp-2 deficiency in T cells does not ameliorate disease outcome and—against the commonly held view—does not impede PD-1 signaling, urging investigation of alternative molecular players.

RESULTS

CD4cre Ptpn11$^{fl/fl}$ Mice Present a Normal T Cell Compartment

First, we characterized the T cell compartment of *CD4cre Ptpn11*$^{fl/fl}$ mice as compared to *CD4cre Ptpn11*$^{wt/wt}$ and *Ptpn11*$^{fl/fl}$ controls. As expected, *Ptpn11* transcript and protein expression were lacking in T cell fractions from *CD4cre Ptpn11*$^{fl/fl}$ mice *ex vivo* and following *in vitro* activation (Figures S1A and S1B). Furthermore, expression of Shp-1 was unaltered, underlying the specificity of Shp-2 deletion (Figures S1A and S1B).

With regard to thymic development, *CD4cre Ptpn11*$^{fl/fl}$ mice did not exhibit differences in thymus cellularity, frequency of CD8 and CD4 double-positive populations, or frequency of single-positive subpopulations (Figures 1A–1C). To exclude that differences in

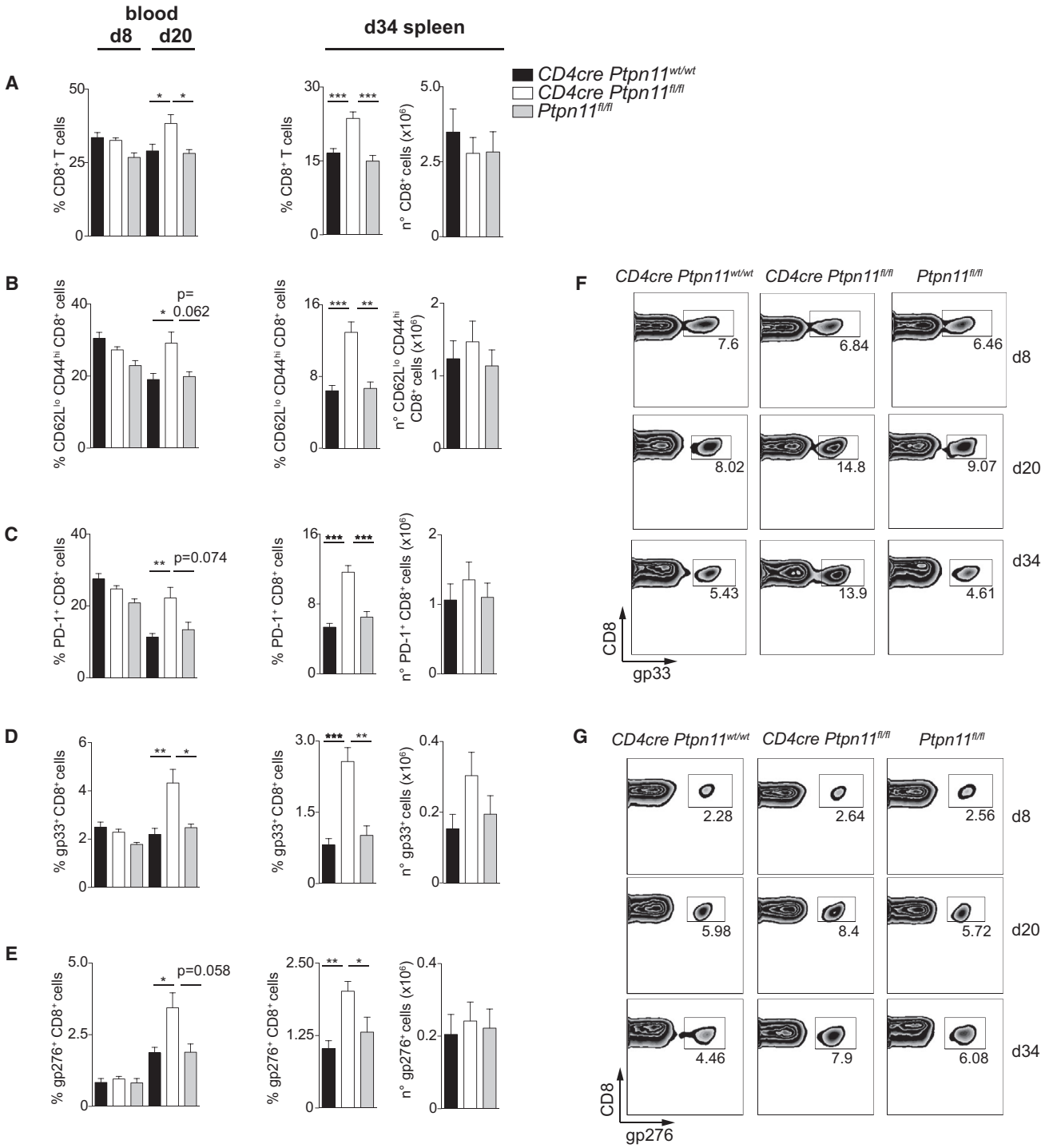

Figure 2. Percentages of *Ptpn11*-Deleted CD8$^+$ T Cells Are Increased upon Chronic Infection

(A) Graphs illustrate percentages of CD8$^+$ T cells at days 8 and 20 p.i. in the blood and percentages and numbers at day 34 p.i. in the spleen of *CD4cre Ptpn11*$^{wt/wt}$, *CD4cre Ptpn11*$^{fl/fl}$, or *Ptpn11*$^{fl/fl}$ mice.

(B and C) Graphs illustrate percentages (among lymphocytes) and numbers of CD44^{high} CD62L^{low} effector (B) or PD-1$^+$ (C) CD8$^+$ T cells.

(D and E) Graphs illustrate percentages (among lymphocytes) and numbers of gp33-specific (gp33$^+$) (D) and gp276-specific (gp276$^+$) (E) CD8$^+$ T cells.

(legend continued on next page)

signaling were compensated for by an altered TCR repertoire, we analyzed thymic development in P14 transgenic mice, which bear a TCR specific for the lymphocytic choriomeningitis virus (LCMV) glycoprotein (gp) 33, and found normal thymic cellularity and frequency of thymocyte subsets (Figures S1C and S1D). In addition, we observed unaltered expression of CD5, CD24, and CD69 and of TCR Vα2 and β chains on double-positive and CD8 single-positive thymocytes (Figures S1E and S1F). Altogether, these results indicate that T cells from *CD4cre Ptpn11*$^{fl/fl}$ mice undergo normal thymic selection.

We next analyzed the peripheral T cell compartment in both spleen and inguinal lymph node. In the spleen, we observed no major differences in the percentages of CD4$^+$ and CD8$^+$ T cells, besides a mild tendency toward increased CD8$^+$ T cells (Figure 1D). Furthermore, the activation state of T lymphocytes, as measured by CD44 and CD62L expression, was unaffected (Figures 1E and 1F). Similar results were obtained for inguinal lymph nodes (Figures S1G–S1I). Altogether, these data indicate that Shp-2 is dispensable for T cell homeostasis in *CD4cre Ptpn11*$^{fl/fl}$ mice.

Ablation of Shp-2 Increases the Frequency of T Cells Specific for Chronic LCMV

With this premise, we challenged mice with LCMV clone 13, which establishes a chronic infection and is therefore widely used as model to study T cell exhaustion. Percentages of *Ptpn11*-deficient CD8$^+$ T cells were similar to controls early after infection (day 8 post-infection [p.i.]) but increased in the chronic phase of the disease (days 20 and 34 p.i.) (Figure 2A). No consistent alterations were observed among CD4$^+$ T cells (Figures S2A and S2B).

We next asked whether the increase of CD8$^+$ T cell percentages in the chronic phase of LCMV infection affected these lymphocytes globally or a particular subset. As shown in Figure 2B, the CD44^{high} CD62L^{low} effector subpopulation, which roughly corresponded to PD-1$^+$ T cells, was augmented in *CD4cre Ptpn11*$^{fl/fl}$ mice (Figure 2C; Figure S2C). In agreement, CD8$^+$ T cells specific for gp33 and gp276 showed normal expansion early after infection and were more abundant in *CD4cre Ptpn11*$^{fl/fl}$ mice at later time points, albeit to different extents (Figures 2D–2G). However, *CD4cre Ptpn11*$^{fl/fl}$ mice had spleens of tendentially reduced cellularity following infection (Figure S2D), rendering the numbers of antiviral CD8$^+$ T cells in *CD4cre Ptpn11*$^{fl/fl}$ mice not increased compared to controls (Figures 2A–2E). T cells bearing only one functional *Ptpn11* allele, from *CD4cre Ptpn11*$^{wt/fl}$ mice, behaved comparably to control cells (Figure S2E). Altogether, these data indicate that *Ptpn11* deletion favored increased frequencies of antiviral T cells.

Shp-2 Limits the Expansion of Exhausted CD8$^+$ T Cells

To gain further insight into the mechanisms leading to increased percentages of *Ptpn11*-deleted effector CD8$^+$ T cells, we took advantage of P14 transgenic T cells. After adoptive cotransfer of *Ptpn11*-deficient and control P14 CD8$^+$ T cells (Figure 3A), we infected recipient mice with LCMV clone 13. Although percentages of *Ptpn11*-deficient and control P14 CD8$^+$ T cells were comparable at day 8 p.i., the former became on average 2.9 times more abundant than the latter during the chronic phase of infection (Figures 3A and 3B). These results proved that accumulation of *Ptpn11*-deficient CD8$^+$ T cells is a cell-intrinsic phenomenon, independent of viral load and thymic output.

The subpopulations of T cells expressing high T-bet and low Eomesodermin levels or the transcription factor Tcf-1 have been shown to renew and sustain the persistent antiviral response (Im et al., 2016; Paley et al., 2012; Utzschneider et al., 2016). However, their frequencies among *Ptpn11*-deficient P14 CD8$^+$ T cells were either unaltered or decreased following chronic infection, while they were high upon acute LCMV infection, irrespectively of the genotype (Figures 3C–3F). These results suggest that the above mechanisms are not responsible for the observed phenotype. We recurrently observed an increased proportion of Ki67$^+$ proliferating cells among *Ptpn11*-deficient P14 T cells (Figures 3G and 3H), indicating that Shp-2 hampered the proliferative capacity of exhausted T cells.

However, expansion of antiviral *Pdcd1*-deficient T cells has been reported to be greater and occur with faster kinetics (Odorizzi et al., 2015). Underlining the divergence in the roles of PD-1 and Shp-2 in exhausted CD8$^+$ T cells, we observed that *Pdcd1*-deficient P14 CD8$^+$ T cells expanded significantly more than their *Ptpn11*-deficient counterparts 11 days after chronic LCMV infection (Figure S3A).

Shp-2 Sustains Polyfunctional CD8$^+$ T Cells in Chronic LCMV Infection

We next asked whether *Ptpn11*-deficient P14 CD8$^+$ T cells from LCMV clone 13-infected mice presented classical exhaustion features. Compared to CD8$^+$ T cells exposed to acute infection, they displayed high levels of inhibitory receptors (Figure 4A). However, while the levels PD-1, lymphocyte-activation gene 3 (Lag3), and T cell immunoreceptor with immunoglobulin (Ig) and ITIM domains (Tigit) were comparable to those of control cells, expression of 2B4 was lower (Figure 4A).

Furthermore, we investigated cytokine production. Because Shp-2 has been implicated in TCR and costimulation or coinhibition signaling (Lee et al., 1998), we restimulated *Ptpn11*-deficient P14 CD8$^+$ T cells with α-CD3 or α-CD3/CD28, enabling control of the engagement of these pathways at the synapse. Although we observed normal degranulation (Figures 4B and 4C) and interferon gamma (IFN-γ) production, IFN-γ/tumor necrosis factor alpha (TNF-α) double-producer cells were underrepresented (Figures 4D and 4E). Similar results were observed upon restimulation with gp33 peptide (Figures S4A–S4D). Concomitant restimulation of P14 T cells from mice infected with acute LCMV

(F and G) Representative flow cytometry plots (gated on CD8$^+$ T cells), as measured in the blood at days 8 and 20 p.i. or in the spleen at day 34 p.i. of gp33-specific (F) or gp276-specific (G) CD8$^+$ T cells.

Results represent mean ± SEM of n = 6–15 mice/group (A–D) or n = 5–8 mice/group (E) are a pool of two independent experiments and are representative of at least three experiments (A–D and F) or two experiments (E and G). Only differences statistically significant in comparison to both controls are shown. *$p \leq 0.05$, **$p \leq 0.01$, ***$p \leq 0.001$; Student's t test. See also Figure S2.

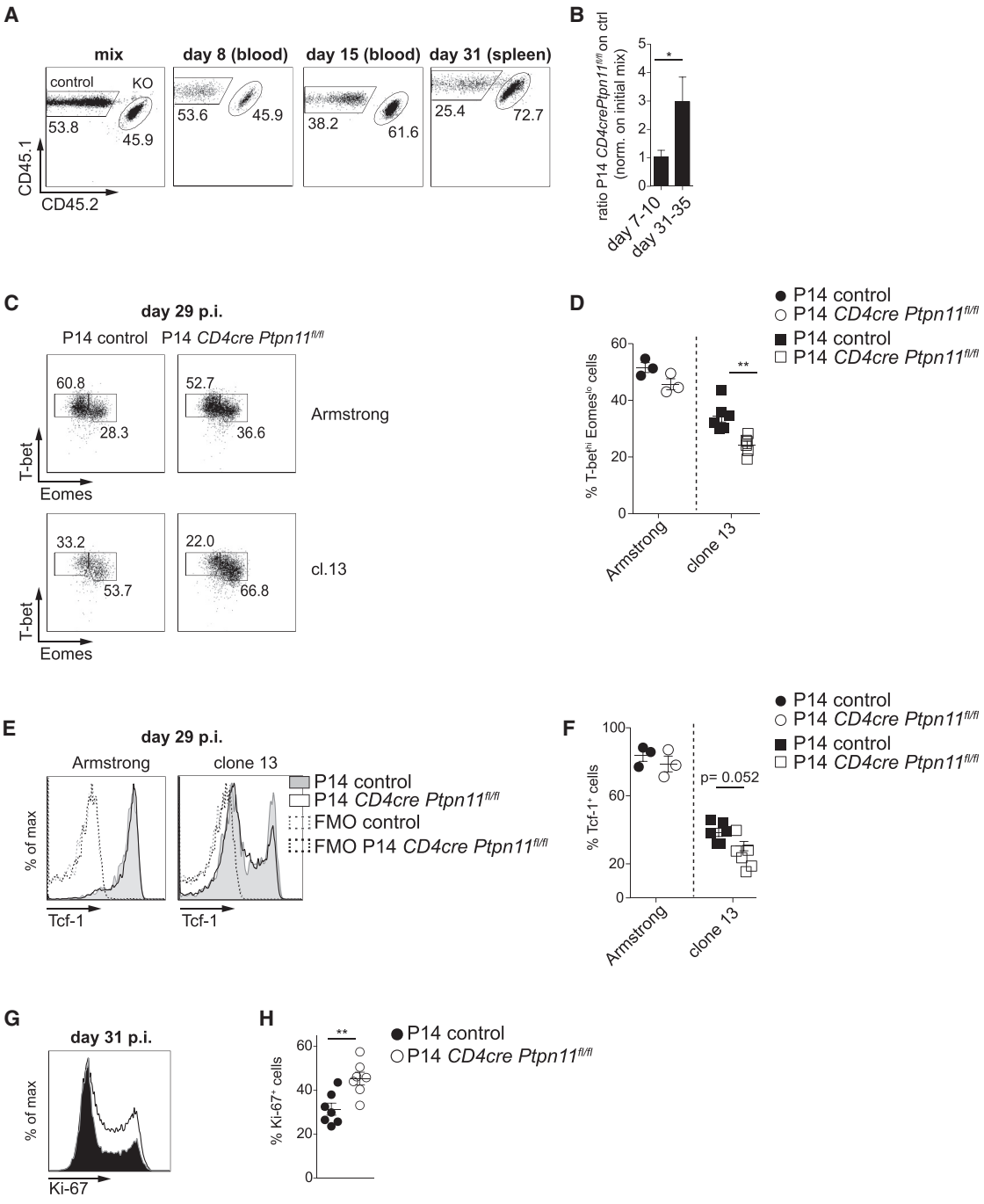

Figure 3. *Ptpn11*-Deficient T Cells Are Increased upon Chronic Infection

Wild-type recipient mice were cotransferred with a 1:1 mix of congenically marked control (which, depending on the experiment, is on a *CD4cre Ptpn11*$^{wt/wt}$, *CD4cre Ptpn11*$^{wt/fl}$, or *Ptpn11*$^{fl/fl}$ background) and *Ptpn11*-deficient (knockout [KO]) (*CD4cre Ptpn11*$^{fl/fl}$ background) P14 CD8$^+$ T cells and infected with LCMV clone 13.

(A) Percentages of KO (CD45.1/2) and control (CD45.1) P14 T cells in the initial mix, in the blood at the indicated days, and in the spleen at day 31 p.i. are shown as representative flow cytometry plots (gated on CD8$^+$ CD45.1$^+$ T cells).

(B) Graph depicts the ratio, normalized to the initial mix, of KO over control P14 T cells at days 7–10 and 31–35 and represents mean ± SEM of the average value of five independent experiments.

(C–F) Representative flow cytometry plots and graphs depict the percentage of T-bet-high and Eomesodermin-low (T-bet^{hi}Eomes^{low}) (C and D) and of Tcf-1 positive (Tcf-1$^+$) (E and F) KO and control P14 T cells 29 days after infection with LCMV clone 13 or Armstrong.

(legend continued on next page)

further evidenced the dysfunctional state of cells from LCMV clone 13-infected animals (Figures S4C and S4D).

Because IL-2 production severely declines upon chronic infection, we tested it following gp33 restimulation at 9 and 29 days p.i. Both control and *Ptpn11*-deficient CD8$^+$ T cells from chronically infected mice produced little IL-2, with the latter synthetizing tendentially lower amounts (Figures 4F and 4G). Altogether, Shp-2-deficient T cells exhibited severe dysfunctional features.

To outline the overall effect of Shp-2 deletion in T cells, we measured viral titers longitudinally in serum and at day 34 p.i. in the kidney of *CD4cre Ptpn11$^{fl/fl}$* and control mice. At all tested time points, we observed comparable virus levels in mice of the different genotypes (Figures S4E and S4F), indicating that the effects of *Ptpn11* deficiency in T cells are not sufficient to substantially alter viral control.

CD4cre Ptpn11$^{fl/fl}$ Mice Show Normal Anticancer Responses and Therapeutic Effects by PD-1 Blockade

Because the antitumoral T cell response is characterized by exhaustion and its modulation is highly relevant for immunotherapy, we investigated the role of Shp-2 in T cells and the combination with α-PD-1 treatment in this context. We chose the immunogenic MC38 adenocarcinoma, which is robustly controlled in *Pdcd1*-deficient mice (Figure S5A) (Juneja et al., 2017). We subcutaneously engrafted *CD4cre Ptpn11$^{fl/fl}$* and control mice with tumor cells. When the tumor was palpable, mice were divided into two groups; one was then injected three times with α-PD-1 antibody, and the other received three injections of isotype control. *CD4cre Ptpn11$^{fl/fl}$* and control mice presented comparable tumor volumes at this stage (Figure S5B). After 30 days, all isotype-treated mice developed large lesions (Figure 5A). To further assess whether alterations in CD4$^+$ T cells indirectly modulated CD8$^+$ T cell anticancer activity in *CD4cre Ptpn11$^{fl/fl}$* mice, we depleted them. This hindered tumor growth in both control and *CD4cre Ptpn11$^{fl/fl}$* mice (Figure S5C) (Yu et al., 2005), indicating that antitumoral CD8$^+$ T cell responses were not inherently different. We thus tested the effects of α-PD-1 treatment. This improved tumor control and mouse survival irrespective of the genotype analyzed, in some cases leading to complete remission (Figures 5B and 5C).

To evaluate whether α-PD-1 treatment exerted the expected effects on intratumoral CD8$^+$ T cells, we examined mice 12 days after engraftment, when therapy started to show efficacy but before numerous tumors were eradicated (Figure S5D). With respect to isotype-treated mice, we detected no substantial differences linked to *Ptpn11* deletion in the frequency of tumor-infiltrating T lymphocytes (Figures 5D; Figure S5E). Furthermore, the proportions of IFN-γ$^+$, PD-1$^+$, 2B4$^+$, and Lag3$^+$ among infiltrating CD8$^+$ T cells were comparable in *CD4cre Ptpn11$^{fl/fl}$* and control mice (Figure 5E; Figure S5F).

α-PD-1 treatment increased the percentages of total and IFN-γ-expressing intratumoral CD8$^+$ T cells in both *CD4cre Ptpn11$^{fl/fl}$* and control mice but reached significance only in the former (Figures 5D and 5E). The efficacy of PD-1 blockade in *CD4cre Ptpn11$^{fl/fl}$* mice revealed that Shp-2 is dispensable for PD-1 signaling in exhausted T cells, indicating that additional players are engaged.

DISCUSSION

Here we addressed the relevance of Shp-2 in exhausted T cells by studying *CD4cre Ptpn11$^{fl/fl}$* mice. In agreement with published studies, we observed that T cells are normal in the absence of Shp-2 (Dong et al., 2015; Liu et al., 2017), rendering these mice suitable for further analyses.

Cotransfer experiments of control and *Ptpn11*-deficient T cells into wild-type mice uncovered enhanced expansion of the latter following chronic viral infection. In agreement, *CD4cre Ptpn11$^{fl/fl}$* mice exhibited increased percentages of virus-specific cytotoxic T cells compared to their control counterparts but no reduction in viral titers. This could be explained by the observation that antiviral T cells were not numerically augmented and exhibited an altered clonal representation, as indicated by the exaggerate proportion of gp33-specific T cells late in the infection. Moreover, we measured decreased frequency of polyfunctional *Ptpn11*-deficient T cells, which are important for viral control.

Along these lines, our results suggested no or a rather positive role for Shp-2 on IL-2 production in the late phase of the infection. However, *in vitro* experiments showed that secretion of this cytokine was suppressed by Shp-2 upon concomitant TCR and PD-1 engagement (Peled et al., 2018; Yokosuka et al., 2012). One limitation of *in vivo* approaches is that these do not enable dissecting the effects of Shp-2 and the pathways in which it operates with the same temporal and molecular accuracy as in *in vitro* settings. However, they answer the central question on the role of this phosphatase in exhausted T cells. In clinically relevant contexts, we thus showed that Shp-2 does not substantially control T cell exhaustion.

The characteristics of *Ptpn11*-deficient T cells differ from those of PD-1 deletion. T cells lacking PD-1 present massive proliferation early after LCMV clone 13 infection, causing excessive immunopathology and mortality of infected mice (Barber et al., 2006; Frebel et al., 2012; Odorizzi et al., 2015); this was not the case for *Ptpn11*-deficient T cells. Furthermore, whereas *Pdcd1*-deficient mice effectively control the immunogenic tumors MC38 and B16, *CD4cre Ptpn11$^{fl/fl}$* mice succumbed with the same kinetics as wild-type controls (Juneja et al., 2017; Woo et al., 2012; Zhang et al., 2013).

Because the role of Shp-2 in regulating PD-1 signaling might have been confounded by additional pathways involving this phosphatase, we tested the response of *CD4cre Ptpn11$^{fl/fl}$* mice to PD-1 blockade. The effects of α-PD-1 treatment were

(G and H) A histogram illustrates Ki67 staining of splenic KO and control P14 T cells at day 31 p.i. (G) and a quantification thereof (H).
Data illustrate mean ± SEM of n = 3 mice/group (Armstrong) (D), and n = 6 mice/group (clone 13) (F), and n = 7 mice/group (H). Results are representative of at least three (A), two (C–F), and three out of five (G and H) independent experiments. Only statistically significant differences are shown. *p ≤ 0.05, **p ≤ 0.01; paired Student's t test (B) and Student's t test (D, F, and H). See also Figure S3.

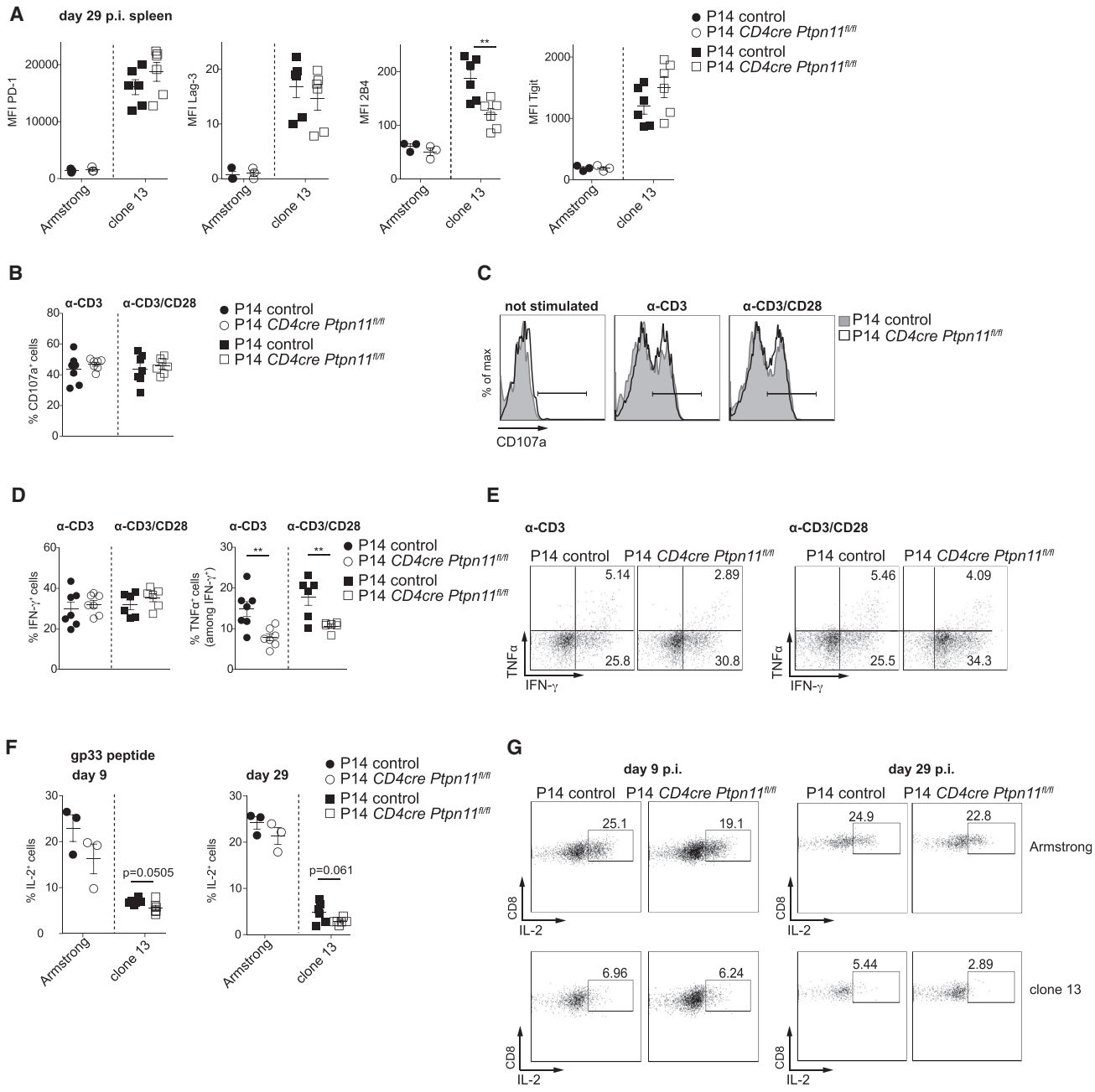

Figure 4. *Ptpn11*-Deficient T Cells Are Dysfunctional upon Chronic Infection

Wild-type recipient mice were cotransferred with a 1:1 mix of congenically marked control and *Ptpn11*-deficient P14 CD8$^+$ T cells and infected with LCMV clone 13.

(A) Graphs depict the geometric mean fluorescence intensity (MFI) of PD-1, Lag3, 2B4, and Tigit on control and *Ptpn11*-deficient P14 CD8$^+$ T cells 29 days following infection with LCMV clone 13 or Armstrong.

(B–E) Splenocytes isolated from infected mice at day 31 p.i. were restimulated with α-CD3 or α-CD3/CD28 and stained for CD107a (B and C), IFN-γ, and TNF-α (D and E). Graphs illustrate frequencies of CD107a$^+$ (B), IFN-γ$^+$, and TNFα$^+$ among IFN-γ$^+$ (D) *Ptpn11*-deficient and control P14 T cells, and representative flow cytometry pictures are shown (C and E).

(F and G) Splenocytes from mice infected with LCMV clone 13 or Armstrong at day 9 or 29 p.i. were restimulated with gp33 peptide and stained for IL-2. Graphs illustrate frequencies of IL-2$^+$ *Ptpn11*-deficient and control P14 T cells (F), and representative flow cytometry pictures are shown (G).

Results depict mean ± SEM of n = 3 (Armstrong) and n = 6 (clone 13) mice/group (A and F), n = 6 or 7 mice/group (B and D) and are representative of at least two independent experiments (A–G). Only statistically significant differences are shown. **p ≤ 0.01; Student's t test (A, B, D, and F). See also Figure S4.

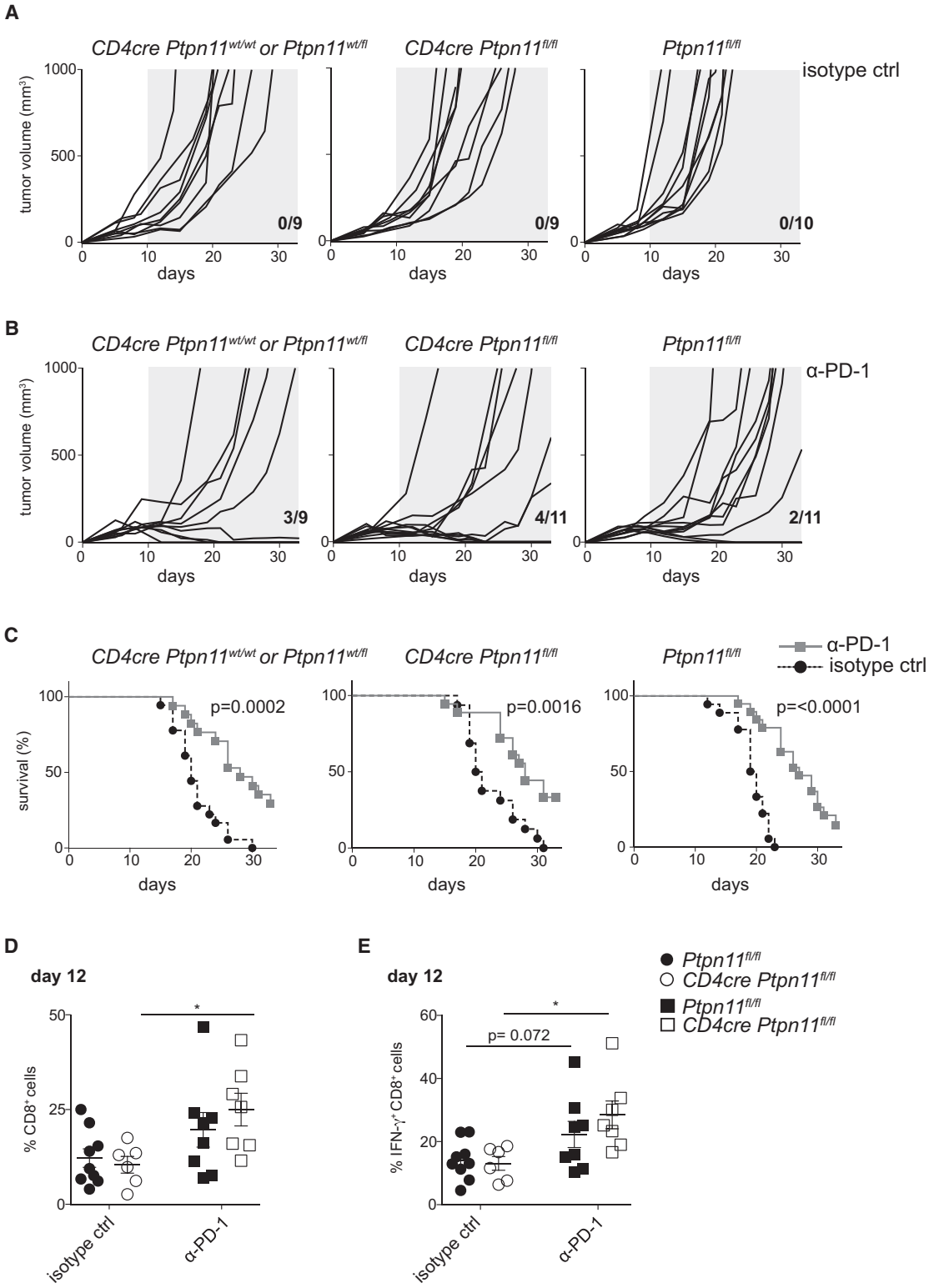

Figure 5. *CD4cre Ptpn11*$^{fl/fl}$ Mice Respond to α-PD-1 Treatment

(A–C) Mice of the indicated genotypes were s.c. inoculated with MC38 cells. (A and B) Tumor growth in individual mice is shown; (A) depicts mice receiving isotype control injections, while (B) shows mice treated with α-PD-1 antibody. The number of mice eradicating the tumor is indicated within the graphs. (C) Survival curves from mice treated as in (A) and (B).

(legend continued on next page)

appreciable, demonstrating that Shp-2 in T cells is dispensable for PD-1-mediated signaling. Our results are in agreement with previous *in vitro* work showing that T cells expressing a dominant-negative form of Shp-2 responded to PD-1 engagement (Salmond et al., 2005). Given the compelling evidence for Shp-2 recruitment to PD-1 (Chemnitz et al., 2004; Hui et al., 2017; Latchman et al., 2001; Lee et al., 1998; Okazaki et al., 2001; Peled et al., 2018; Sheppard et al., 2004; Yamamoto et al., 2008; Yokosuka et al., 2012), we propose that redundant mechanisms mediate this inhibitory signaling. The cytoplasmic tail of PD-1 is dephosphorylated by Shp-2 as part of a feedback loop (Hui et al., 2017; Yokosuka et al., 2012). This suggests accumulation of phosphorylated PD-1 and recruitment of other phosphatases to be enhanced in the absence of Shp-2.

The development of Shp-2 inhibitors is key to improve the clinical management of several malignancies (Chen et al., 2016; Lan et al., 2015). Together with the expanding use of immunotherapeutic approaches, we felt that a deeper understanding of the role of Shp-2 in T cell exhaustion was essential. While we showed that Shp-2 deletion in T cells failed to provide an advantage in controlling growth of immunogenic tumors, this did not hinder the therapeutic effects of PD-1 blockade, supporting the prospect of combination therapies.

Despite the increasing use of inhibitory receptor blocking antibodies in patients, our findings highlight how the engaged signaling pathways remain poorly understood. We demonstrate that Shp-2 is dispensable for imprinting the global dysfunctional state of T cells *in vivo*. Our results are relevant for translational research and encourage further investigations that will uncover novel targets for anticancer therapies.

EXPERIMENTAL PROCEDURES

Additional information on the experimental procedures used is included in the Supplemental Information.

Mice

Ptpn11$^{fl/fl}$ mice (Grossmann et al., 2009) were on a mixed C57BL/6 background and crossed at least six additional times on C57BL/6 in the animal facility of the University of Lausanne. *CD4cre* deleter strain was from Jackson Laboratory. *Ptpn11*$^{fl/fl}$ control mice were littermates of *CD4cre Ptpn11*$^{fl/fl}$ mice. CD45.1^{+} P14αβ mice (Pircher et al., 1990) on a C57BL/6 background were crossed onto *CD4cre Ptpn11*$^{fl/fl}$ and onto a *Pdcd1*-deficient background (Nishimura et al., 1998) in the animal facility of the University of Lausanne. Unless otherwise specified, male and female 6- to 12-week-old mice were used in different experiments with appropriate sex- and age-matched controls.

LCMV Infection

LCMV clone 13 and Armstrong strain were propagated as previously described (Ludigs et al., 2016). Frozen stocks were diluted in PBS; 2 × 10^6 plaque-forming units of LCMV (clone 13) were injected intravenously or 2 × 10^5 plaque-forming units (Armstrong) were injected intraperitoneally. Transgenic P14 CD8^{+} T cells were isolated with α-CD8a magnetic beads (Miltenyi Biotec). Unless otherwise specified, 2 × 10^3–4 × 10^3 control and an equal number of *CD4cre Ptpn11*$^{fl/fl}$ P14 CD8^{+} T cells were intravenously cotransferred into naive C57BL/6 mice, which were infected on the same day. Viral titer analysis was performed as previously described (Ludigs et al., 2016).

Engrafted Tumors

The colon adenocarcinoma cell line MC38 was grown in monolayer in DMEM supplemented with 10% fetal calf serum (FCS), 100 U/mL of penicillin, and 100 μg/mL of streptomycin. Tumor cells were harvested with 0.05% trypsin, washed, and resuspended in PBS for injection. 5 × 10^5 tumor cells were injected subcutaneously (s.c.) in the flank. Tumor volume was calculated using the formula $V = (L \times l^2)/2$, where L is the widest diameter and l is the smallest diameter. Animals were sacrificed when tumor volume reached 1,000 mm^3. Depending on the experiment, starting 5–7 days post-tumor engraftment, when tumors were palpable, mice were treated intraperitoneally with α-PD-1 (RMP1–RMP14, BioXcell) or isotype control (2A3, BioXcell). The treatment was repeated two times at an interval of 3–4 days for a total of three injections of 200 μg/mouse.

Statistical Analysis

Statistical analyses were performed using Prism software (GraphPad v.5.0). Student's t test (unpaired, two-tailed) was used to compare differences between experimental groups. Differences were considered significant when *$p < 0.05$, very significant when **$p < 0.01$, and highly significant when ***$p < 0.001$. For survival, comparisons are by log-rank (Mantel-Cox) test.

Study Approval

Mouse studies were approved by the Veterinary Office regulations of the State of Vaud, Switzerland.

SUPPLEMENTAL INFORMATION

Supplemental Information includes Supplemental Experimental Procedures and five figures and can be found with this article online at https://doi.org/10.1016/j.celrep.2018.03.026.

ACKNOWLEDGMENTS

We thank T. Honjo, Kyoto University, Kyoto; O. Demaria, Innate Pharma, Marseille; O. Donzé, Adipogen, Lausanne; P.C. Ho, W. Held, M. Charmoy, and A. Wilson, Ludwig Center for Cancer Research, Lausanne; and K. Schäuble and S. Luther, University of Lausanne, for reagents and advice. Studies in the group of G.G. are funded by the Swiss National Science Foundation (PP00P3_139094 and PP00P3_165833) and the European Research Council (ERC) (StG310890). The D.Z. lab is supported by the ERC (337043-ProtecTC). The E.V. lab is supported by the ERC (694502) under the European Union's Horizon 2020 research and innovation program, Agence Nationale de la Recherche, Innate Pharma, MSDAvenir, Ligue Nationale contre le Cancer (Equipe labelisée "La Ligue"), and Marseille-Immunopole.

AUTHOR CONTRIBUTIONS

G.R., C.N., A.T.D., C.R.B., N.P.F., and L.M. performed the experiments; F.A., D.Z., W.B., and E.V. shared protocols, reagents, and advice; and G.R. and G.G. designed the research, analyzed the data, and wrote the manuscript.

(D and E) 12 days following MC38 tumor inoculation and the day after the third injection of α-PD-1 antibody or isotype control, mice were sacrificed and tumor-infiltrating T cells were analyzed. Graphs depict percentages of CD8^{+} (CD8^{+} CD3^{+}) (D) and CD8^{+} IFN-γ-producing (E) infiltrating T cells among hematopoietic cells.

Results depict n = 9–11 mice/group (A and B), n = 16–19 mice/group (C), and are a pool of two (A and B) or four experiments (C). For survival, comparisons are by log-rank (Mantel-Cox) test; isotype-treated *CD4cre Ptpn11*$^{fl/fl}$ and *CD4cre Ptpn11*$^{wt/wt}$ or $^{wt/fl}$ mice, p = 0.2511; isotype-treated *CD4cre Ptpn11*$^{fl/fl}$ and *Ptpn11*$^{fl/fl}$ mice, p = 0.0205; α-PD-1-treated *CD4cre Ptpn11*$^{fl/fl}$ and *CD4cre Ptpn11*$^{wt/wt}$ or $^{wt/fl}$ mice, p = 0.7975; α-PD-1-treated *CD4cre Ptpn11*$^{fl/fl}$ and *Ptpn11*$^{fl/fl}$ mice, p = 0.2975. (D and E) Results depict mean ± SEM of n = 6-9 mice/group and are a pool of two experiments. Only statistically significant differences are shown. *$p \leq 0.05$; Student's t test. See also Figure S5.

DECLARATION OF INTERESTS

E.V. is a cofounder, shareholder, and employee of Innate Pharma. The other authors declare no competing interests.

Received: July 20, 2017
Revised: January 15, 2018
Accepted: March 7, 2018
Published: April 3, 2018

REFERENCES

Barber, D.L., Wherry, E.J., Masopust, D., Zhu, B., Allison, J.P., Sharpe, A.H., Freeman, G.J., and Ahmed, R. (2006). Restoring function in exhausted CD8 T cells during chronic viral infection. Nature *439*, 682–687.

Chan, G., Kalaitzidis, D., and Neel, B.G. (2008). The tyrosine phosphatase Shp2 (PTPN11) in cancer. Cancer Metastasis Rev. *27*, 179–192.

Chemnitz, J.M., Parry, R.V., Nichols, K.E., June, C.H., and Riley, J.L. (2004). SHP-1 and SHP-2 associate with immunoreceptor tyrosine-based switch motif of programmed death 1 upon primary human T cell stimulation, but only receptor ligation prevents T cell activation. J. Immunol. *173*, 945–954.

Chen, Y.P., LaMarche, M.J., Chan, H.M., Fekkes, P., Garcia-Fortanet, J., Acker, M.G., Antonakos, B., Chen, C.H., Chen, Z., Cooke, V.G., et al. (2016). Allosteric inhibition of SHP2 phosphatase inhibits cancers driven by receptor tyrosine kinases. Nature *535*, 148–152.

Cunnick, J.M., Mei, L., Doupnik, C.A., and Wu, J. (2001). Phosphotyrosines 627 and 659 of Gab1 constitute a bisphosphoryl tyrosine-based activation motif (BTAM) conferring binding and activation of SHP2. J. Biol. Chem. *276*, 24380–24387.

Dong, B., Gao, Y., Zheng, X., Gao, G., Gu, H., Chen, X., and Zhang, J. (2015). T cell activation is reduced by the catalytically inactive form of protein tyrosine phosphatase SHP-2. Int. J. Clin. Exp. Med. *8*, 6568–6577.

Ekman, S., Kallin, A., Engstrom, U., Heldin, C.H., and Ronnstrand, L. (2002). SHP-2 is involved in heterodimer specific loss of phosphorylation of Tyr771 in the PDGF beta-receptor. Oncogene *21*, 1870–1875.

Frebel, H., Nindl, V., Schuepbach, R.A., Braunschweiler, T., Richter, K., Vogel, J., Wagner, C.A., Loffing-Cueni, D., Kurrer, M., Ludewig, B., et al. (2012). Programmed death 1 protects from fatal circulatory failure during systemic virus infection of mice. J. Exp. Med. *209*, 2485–2499.

Gadina, M., Stancato, L.M., Bacon, C.M., Larner, A.C., and O'Shea, J.J. (1998). Involvement of SHP-2 in multiple aspects of IL-2 signaling: evidence for a positive regulatory role. J. Immunol. *160*, 4657–4661.

Grossmann, K.S., Wende, H., Paul, F.E., Cheret, C., Garratt, A.N., Zurborg, S., Feinberg, K., Besser, D., Schulz, H., Peles, E., et al. (2009). The tyrosine phosphatase Shp2 (PTPN11) directs Neuregulin-1/ErbB signaling throughout Schwann cell development. Proc. Natl. Acad. Sci. USA *106*, 16704–16709.

Hui, E., Cheung, J., Zhu, J., Su, X., Taylor, M.J., Wallweber, H.A., Sasmal, D.K., Huang, J., Kim, J.M., Mellman, I., et al. (2017). T cell costimulatory receptor CD28 is a primary target for PD-1-mediated inhibition. Science *355*, 1428–1433.

Im, S.J., Hashimoto, M., Gerner, M.Y., Lee, J., Kissick, H.T., Burger, M.C., Shan, Q., Hale, J.S., Lee, J., Nasti, T.H., et al. (2016). Defining CD8+ T cells that provide the proliferative burst after PD-1 therapy. Nature *537*, 417–421.

Juneja, V.R., McGuire, K.A., Manguso, R.T., LaFleur, M.W., Collins, N., Haining, W.N., Freeman, G.J., and Sharpe, A.H. (2017). PD-L1 on tumor cells is sufficient for immune evasion in immunogenic tumors and inhibits CD8 T cell cytotoxicity. J. Exp. Med. *214*, 895–904.

Kwon, J., Qu, C.K., Maeng, J.S., Falahati, R., Lee, C., and Williams, M.S. (2005). Receptor-stimulated oxidation of SHP-2 promotes T-cell adhesion through SLP-76-ADAP. EMBO J. *24*, 2331–2341.

Lan, L., Holland, J.D., Qi, J., Grosskopf, S., Rademann, J., Vogel, R., Gyorffy, B., Wulf-Goldenberg, A., and Birchmeier, W. (2015). Shp2 signaling suppresses senescence in PyMT-induced mammary gland cancer in mice. EMBO J. *34*, 1493–1508.

Latchman, Y., Wood, C.R., Chernova, T., Chaudhary, D., Borde, M., Chernova, I., Iwai, Y., Long, A.J., Brown, J.A., Nunes, R., et al. (2001). PD-L2 is a second ligand for PD-1 and inhibits T cell activation. Nat. Immunol. *2*, 261–268.

Lee, K.M., Chuang, E., Griffin, M., Khattri, R., Hong, D.K., Zhang, W., Straus, D., Samelson, L.E., Thompson, C.B., and Bluestone, J.A. (1998). Molecular basis of T cell inactivation by CTLA-4. Science *282*, 2263–2266.

Liu, W., Guo, W., Shen, L., Chen, Z., Luo, Q., Luo, X., Feng, G., Shu, Y., Gu, Y., Xu, Q., et al. (2017). T lymphocyte SHP2-deficiency triggers anti-tumor immunity to inhibit colitis-associated cancer in mice. Oncotarget *8*, 7586–7597.

Ludigs, K., Jandus, C., Utzschneider, D.T., Staehli, F., Bessoles, S., Dang, A.T., Rota, G., Castro, W., Zehn, D., Vivier, E., et al. (2016). NLRC5 shields T lymphocytes from NK-cell-mediated elimination under inflammatory conditions. Nat. Commun. *7*, 10554.

Miah, S.M.S., Jayasuriya, C.T., Salter, A.I., Reilly, E.C., Fugere, C., Yang, W., Chen, Q., and Brossay, L. (2017). Ptpn11 deletion in CD4+ cells does not affect T cell development and functions but causes cartilage tumors in a T cell-independent manner. Front. Immunol. *8*, 1326.

Nguyen, T.V., Ke, Y., Zhang, E.E., and Feng, G.S. (2006). Conditional deletion of Shp2 tyrosine phosphatase in thymocytes suppresses both pre-TCR and TCR signals. J. Immunol. *177*, 5990–5996.

Nishimura, H., Minato, N., Nakano, T., and Honjo, T. (1998). Immunological studies on PD-1 deficient mice: implications of PD-1 as a negative regulator for B cell responses. Int. Immunol. *10*, 1563–1572.

Noguchi, T., Matozaki, T., Horita, K., Fujioka, Y., and Kasuga, M. (1994). Role of SH-PTP2, a protein-tyrosine phosphatase with Src homology 2 domains, in insulin-stimulated Ras activation. Mol. Cell. Biol. *14*, 6674–6682.

Odorizzi, P.M., Pauken, K.E., Paley, M.A., Sharpe, A., and Wherry, E.J. (2015). Genetic absence of PD-1 promotes accumulation of terminally differentiated exhausted CD8+ T cells. J. Exp. Med. *212*, 1125–1137.

Okazaki, T., Maeda, A., Nishimura, H., Kurosaki, T., and Honjo, T. (2001). PD-1 immunoreceptor inhibits B cell receptor-mediated signaling by recruiting src homology 2-domain-containing tyrosine phosphatase 2 to phosphotyrosine. Proc. Natl. Acad. Sci. USA *98*, 13866–13871.

Paley, M.A., Kroy, D.C., Odorizzi, P.M., Johnnidis, J.B., Dolfi, D.V., Barnett, B.E., Bikoff, E.K., Robertson, E.J., Lauer, G.M., Reiner, S.L., et al. (2012). Progenitor and terminal subsets of CD8+ T cells cooperate to contain chronic viral infection. Science *338*, 1220–1225.

Pauken, K.E., and Wherry, E.J. (2015). Overcoming T cell exhaustion in infection and cancer. Trends Immunol. *36*, 265–276.

Peled, M., Tocheva, A.S., Sandigursky, S., Nayak, S., Philips, E.A., Nichols, K.E., Strazza, M., Azoulay-Alfaguter, I., Askenazi, M., Neel, B.G., et al. (2018). Affinity purification mass spectrometry analysis of PD-1 uncovers SAP as a new checkpoint inhibitor. Proc. Natl. Acad. Sci. USA. *115*, E468–E477.

Pircher, H., Moskophidis, D., Rohrer, U., Bürki, K., Hengartner, H., and Zinkernagel, R.M. (1990). Viral escape by selection of cytotoxic T cell-resistant virus variants in vivo. Nature *346*, 629–633.

Prahallad, A., Heynen, G.J., Germano, G., Willems, S.M., Evers, B., Vecchione, L., Gambino, V., Lieftink, C., Beijersbergen, R.L., Di Nicolantonio, F., et al. (2015). PTPN11 is a central node in intrinsic and acquired resistance to targeted cancer drugs. Cell Rep. *12*, 1978–1985.

Salmond, R.J., Huyer, G., Kotsoni, A., Clements, L., and Alexander, D.R. (2005). The src homology 2 domain-containing tyrosine phosphatase 2 regulates primary T-dependent immune responses and Th cell differentiation. J. Immunol. *175*, 6498–6508.

Sheppard, K.A., Fitz, L.J., Lee, J.M., Benander, C., George, J.A., Wooters, J., Qiu, Y., Jussif, J.M., Carter, L.L., Wood, C.R., et al. (2004). PD-1 inhibits T-cell receptor induced phosphorylation of the ZAP70/CD3zeta signalosome and downstream signaling to PKCtheta. FEBS Lett. *574*, 37–41.

Siminovitch, K.A., and Neel, B.G. (1998). Regulation of B cell signal transduction by SH2-containing protein-tyrosine phosphatases. Semin. Immunol. *10*, 329–347.

Speiser, D.E., Utzschneider, D.T., Oberle, S.G., Munz, C., Romero, P., and Zehn, D. (2014). T cell differentiation in chronic infection and cancer: functional adaptation or exhaustion? Nat. Rev. Immunol. *14*, 768–774.

Tajan, M., de Rocca Serra, A., Valet, P., Edouard, T., and Yart, A. (2015). SHP2 sails from physiology to pathology. Eur. J. Med. Genet. *58*, 509–525.

Topalian, S.L., Drake, C.G., and Pardoll, D.M. (2015). Immune checkpoint blockade: a common denominator approach to cancer therapy. Cancer Cell *27*, 450–461.

Utzschneider, D.T., Charmoy, M., Chennupati, V., Pousse, L., Ferreira, D.P., Calderon-Copete, S., Danilo, M., Alfei, F., Hofmann, M., Wieland, D., et al. (2016). T cell factor 1-expressing memory-like CD8(+) T cells sustain the immune response to chronic viral infections. Immunity *45*, 415–427.

Woo, S.R., Turnis, M.E., Goldberg, M.V., Bankoti, J., Selby, M., Nirschl, C.J., Bettini, M.L., Gravano, D.M., Vogel, P., Liu, C.L., et al. (2012). Immune inhibitory molecules LAG-3 and PD-1 synergistically regulate T-cell function to promote tumoral immune escape. Cancer Res. *72*, 917–927.

Yamamoto, R., Nishikori, M., Kitawaki, T., Sakai, T., Hishizawa, M., Tashima, M., Kondo, T., Ohmori, K., Kurata, M., Hayashi, T., et al. (2008). PD-1-PD-1 ligand interaction contributes to immunosuppressive microenvironment of Hodgkin lymphoma. Blood *111*, 3220–3224.

Yokosuka, T., Takamatsu, M., Kobayashi-Imanishi, W., Hashimoto-Tane, A., Azuma, M., and Saito, T. (2012). Programmed cell death 1 forms negative costimulatory microclusters that directly inhibit T cell receptor signaling by recruiting phosphatase SHP2. J. Exp. Med. *209*, 1201–1217.

Yu, P., Lee, Y., Liu, W., Krausz, T., Chong, A., Schreiber, H., and Fu, Y.X. (2005). Intratumor depletion of CD4+ cells unmasks tumor immunogenicity leading to the rejection of late-stage tumors. J. Exp. Med. *201*, 779–791.

Zhang, T., Guo, W., Yang, Y., Liu, W., Guo, L., Gu, Y., Shu, Y., Wang, L., Wu, X., Hua, Z., et al. (2013). Loss of SHP-2 activity in CD4+ T cells promotes melanoma progression and metastasis. Sci. Rep. *3*, 2845.

Zhang, J., Zhang, F., and Niu, R. (2015). Functions of Shp2 in cancer. J. Cell. Mol. Med. *19*, 2075–2083.

Cell Reports, Volume *23*

Supplemental Information

Shp-2 Is Dispensable for Establishing T Cell Exhaustion and for PD-1 Signaling *In Vivo*

Giorgia Rota, Charlène Niogret, Anh Thu Dang, Cristina Ramon Barros, Nicolas Pierre Fonta, Francesca Alfei, Leonor Morgado, Dietmar Zehn, Walter Birchmeier, Eric Vivier, and Greta Guarda

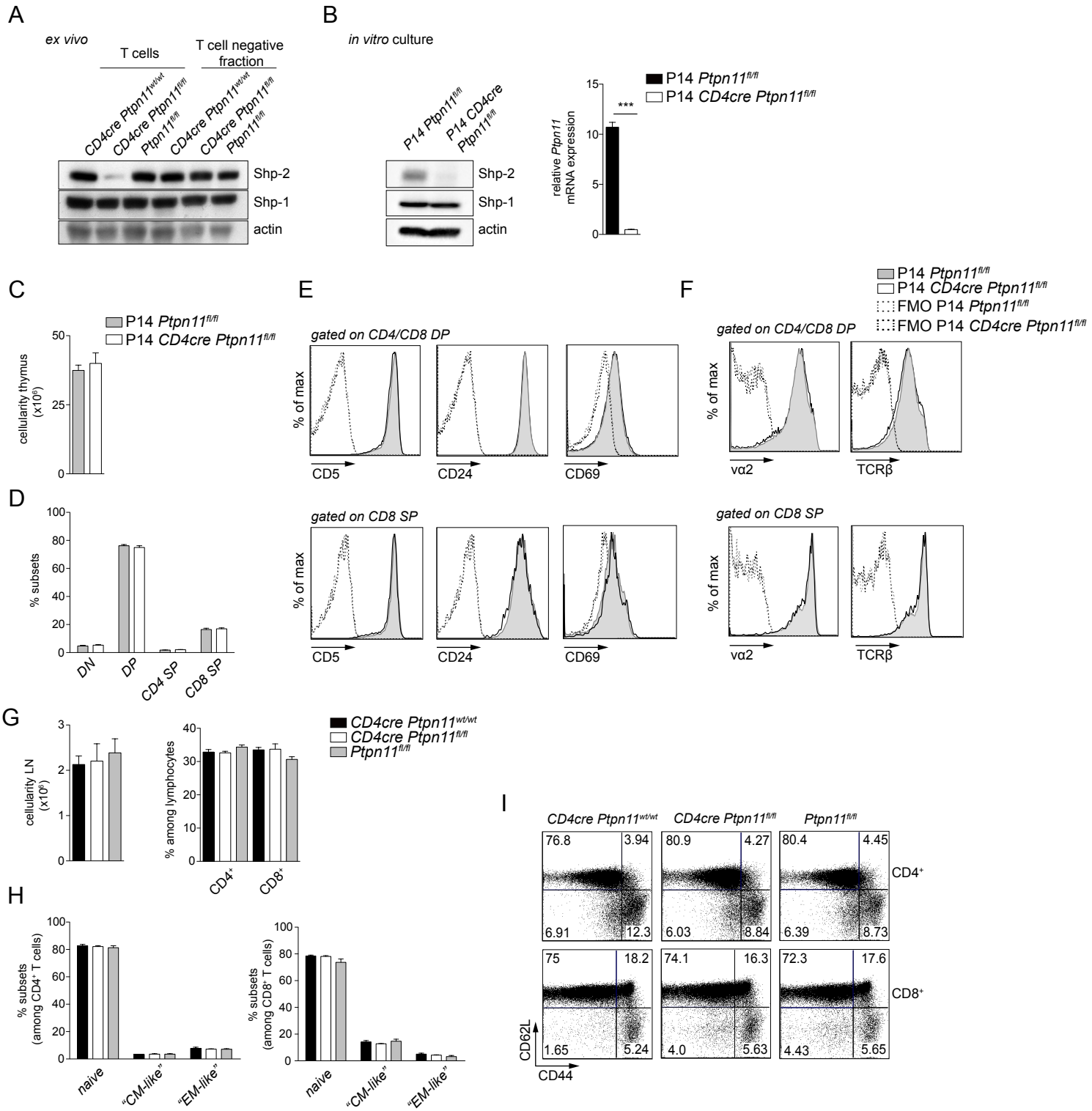

Figure S1. Shp-2 is deleted in T cells and *CD4cre Ptpn11$^{fl/fl}$* mice show normal T cell selection and peripheral homeostasis . Related to Figure 1. A) Total T cells were enriched from spleens of *CD4cre Ptpn11$^{wt/wt}$*, *CD4cre Ptpn11$^{fl/fl}$* and *Ptpn11$^{fl/fl}$* mice. The remaining fraction is indicated as T cell-negative. Expression of Shp-2 or Shp-1 was tested by immunoblot in cell lysates from the indicated subsets, actin used as loading control. T cell purity was over 90%, whereas T cell contamination in T cell-depleted spenocytes less than 5%. B) CD8$^+$ T cells were enriched from spleens of P14 transgenic *CD4cre Ptpn11$^{fl/fl}$* and *Ptpn11$^{fl/fl}$* mice, with a purity of over 97%. Cell were activated with plastic-bound α-CD3 and α-CD28 (1μg/ml each, in the presence of 10 ng/ml IL-2) for 48 hours and cultured for additional 48 hours (in the presence of 20 ng/ml IL-2). Cells were then collected and expression of Shp-2 or Shp-1 was tested by immunoblot (left panel) and abundance of *Ptpn11* mRNA determined by quantitative RT-PCR (relative to *Polr2a*; right panel). Quantitative RT-PCR data represent mean ± SD of n=3 technical replicates and are representative of at least two independent experiments. C-F) Analysis of thymi from P14-transgenic *CD4cre Ptpn11$^{fl/fl}$* and *Ptpn11$^{fl/fl}$* mice. C and D) Cellularity (C) and percentages of DN, DP, and SP thymocytes among lineage-negative lymphocytes (D) are depicted. E and F) A representative histogram illustrates the levels of CD5, CD24, and CD69 (E) and of Vα2 and TCRβ (F) on DP and CD8 SP. G) Inguinal lymph nodes (LNs) cellularity and percentages of CD4$^+$ (CD4$^+$ CD3$^+$) and CD8$^+$ (CD8$^+$ CD3$^+$) T cells (gated on lymphocytes) in *CD4cre Ptpn11$^{wt/wt}$*, *CD4cre Ptpn11$^{fl/fl}$*, and *Ptpn11$^{fl/fl}$* mice are illustrated. H and I) Percentages of naïve (CD44$^{low\text{-}int}$ CD62L^{high}), "CM-like" (CD44^{high} CD62L^{high}), and "EM-like" (CD44^{high} CD62L^{low}) CD4$^+$ and CD8$^+$ T lymphocytes in the iLNs of the afore-mentioned mice (H) and a representative flow cytometry plot of CD62L and CD44 expression (I) are depicted. Results represent mean ± SEM of n=4 mice/ group (C and D) and of n=3-5 mice/group (G and H) and are representative of two (C-F) or at least two (G-I) independent experiments. Only statistically significant differences are shown (B-D, G and H); Student's t-test; ***p ≤ 0.001

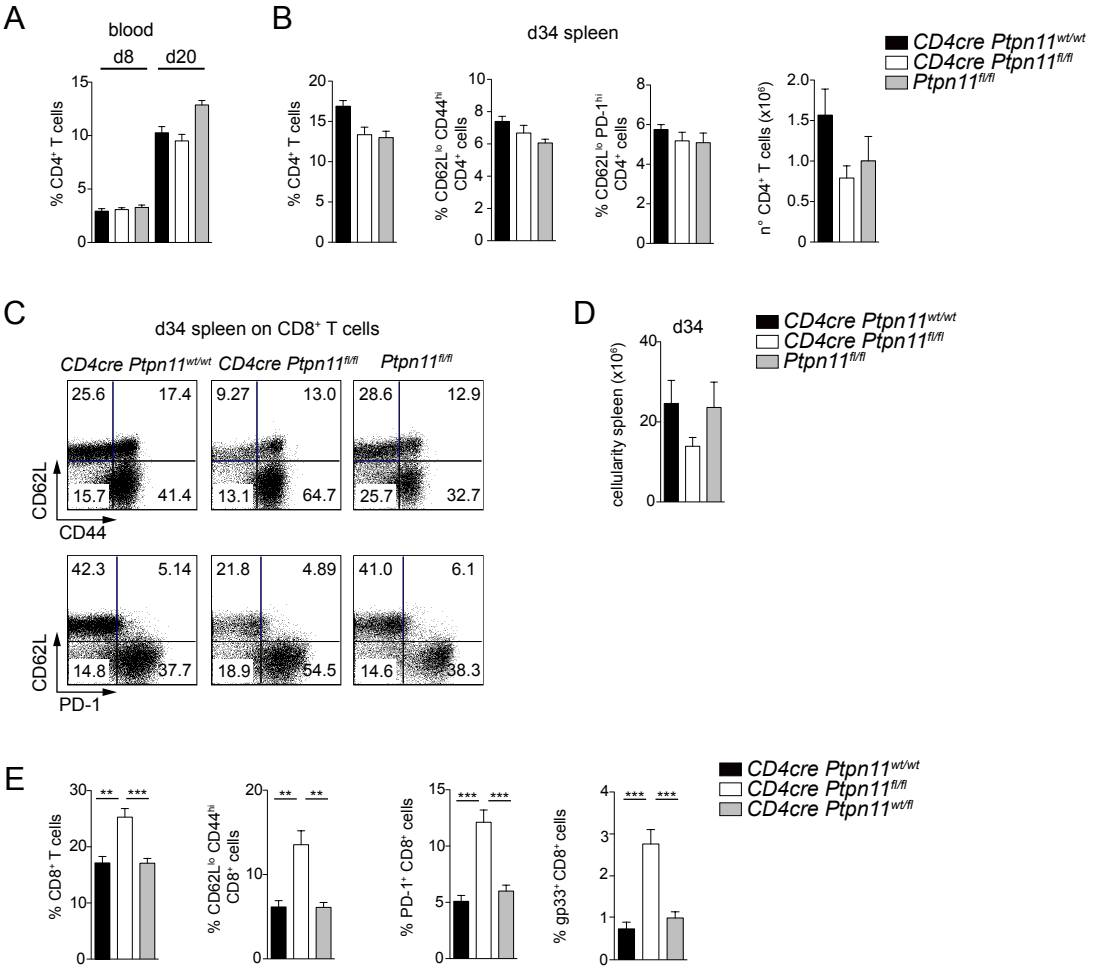

Figure S2. Characterization of T cells in *CD4cre Ptpn11$^{fl/fl}$* mice during chronic LCMV. Related to Figure 2
A) Graph illustrates percentages of CD4$^+$ T cells at day 8 and 20 p.i. in blood of *CD4cre Ptpn11$^{wt/wt}$*, *CD4cre Ptpn11$^{fl/fl}$* and *Ptpn11$^{fl/fl}$* mice. B) Graphs depict percentages and numbers of CD4$^+$ T cells, percentages of CD62L low CD44 high (CD62L^{lo} CD44^{hi}), and of CD62L low PD-1 high (CD62L^{lo} PD-1^{hi}) CD4$^+$ T cells at day 34 p.i. in the spleen of the afore-mentioned mice. C) Representative flow cytometry plots of CD62L/CD44 or CD62L/PD-1 expression on CD8$^+$ T cells at day 34 p.i. in the spleen. D) Graph shows spleen cellularity of *CD4cre Ptpn11$^{wt/wt}$*, *CD4cre Ptpn11$^{fl/fl}$* and *Ptpn11$^{fl/fl}$* mice at day 34 p.i.. E) Graphs illustrate percentages of CD8$^+$, CD44high CD62Llow effector, PD1$^+$, and gp33-specific (gp33$^+$) T cells among lymphocytes in the spleen of *CD4cre Ptpn11$^{wt/wt}$*, *CD4cre Ptpn11$^{fl/fl}$*, and *CD4cre Ptpn11$^{wt/fl}$* mice at day 34 p.i.. A, B, D, and E) Results are a pool of two independent experiments, and mean ± SEM of n=6-15 (A), n=6-12 (B and D), n=7-8 (E) mice/group. Only differences statistically significant in comparison to both controls are shown; **p ≤ 0.01, ***p ≤ 0.001; Student's t-test

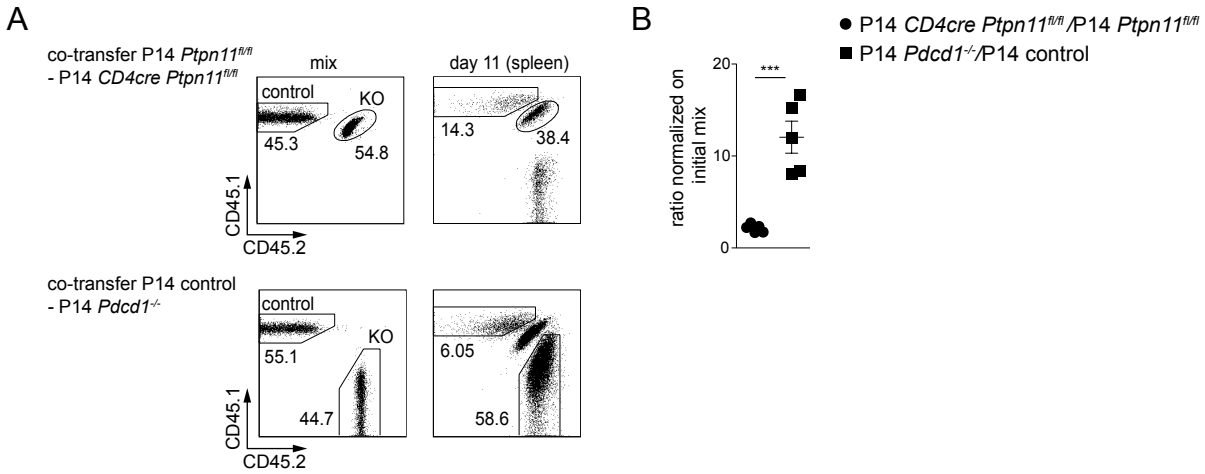

Figure S3. *Ptnp11*- and *Pdcd1*- deficient T cells show profound differences in expansion upon chronic LCMV. Related to Figure 3. Wild type recipient mice (CD45.2) were co-transferred with a mix of 400 control (*Ptpn11*$^{fl/fl}$, CD45.1) and 400 *Ptpn11*-deficient (KO; *CD4cre Ptpn11*$^{fl/fl}$, CD45.1/2) P14 CD8$^+$ T cells and infected with LCMV clone 13. In parallel, wild type mice (CD45.1/2) were co-transferred with a mix of 400 control (CD45.1) and 400 *Pdcd1*-deficient (KO; CD45.2) P14 CD8$^+$ T cells and infected with LCMV clone 13. A) Percentages of KO and control P14 T cells in the initial mix and in the spleen at day 11 p.i. are shown as a representative flow cytometry plot (gated on Va2$^+$ CD8$^+$ T cells). B) The graph depicts the ratio of *Ptpn11*- or *Pdcd1*- deficient over control (normalized to the initial mix) at day 11 in individual mice (n=5 mice/group); Only statistically significant differences are shown; ***$p \leq 0.001$; Student's t-test.

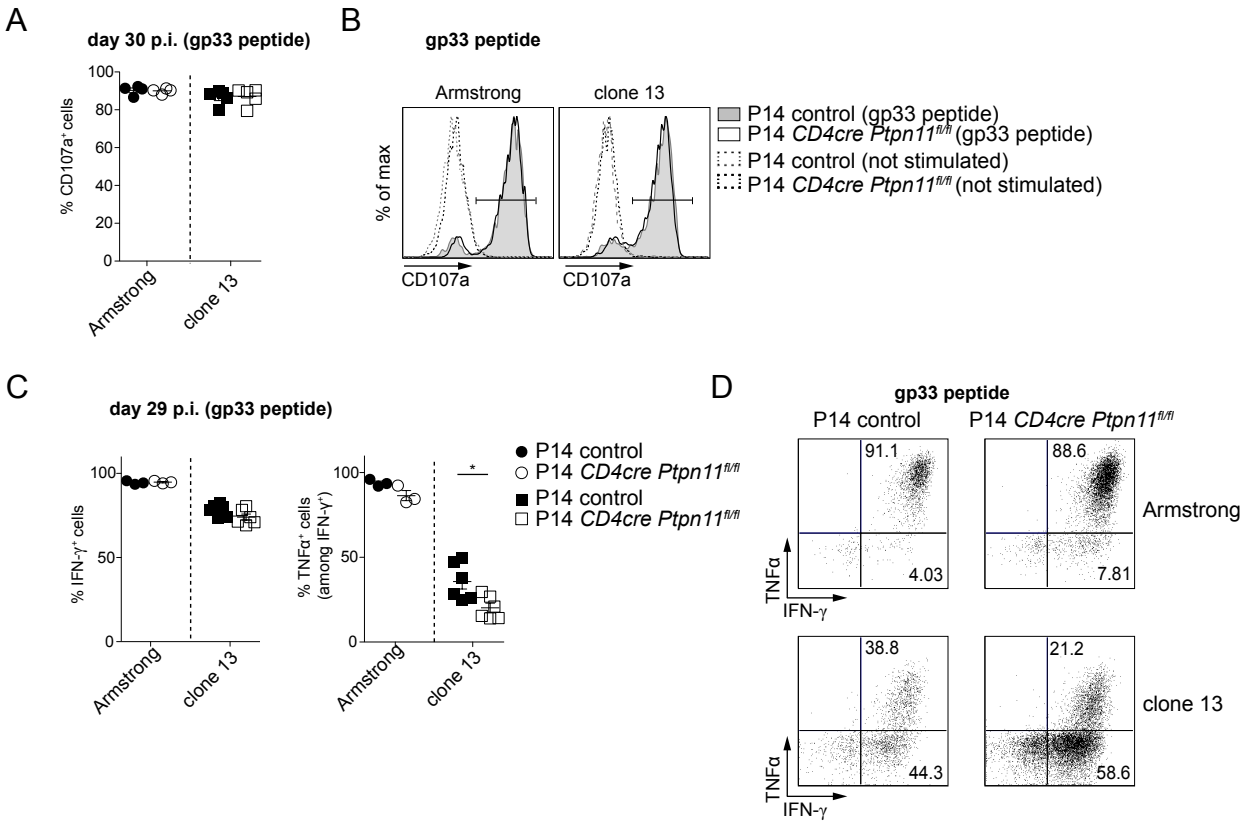

Figure S4. Functional characterization of *Ptnp11*-deficient T cells during chronic LCMV. Related to Figure 4
A-D) Wild type recipient mice were co-transferred with a 1:1 mix of congenically-marked control (*CD4cre Ptpn11*$^{wt/wt}$) and *Ptpn11*-deficient P14 CD8$^+$ T cells and infected with LCMV clone 13 or Armstrong, as a control. A-D) Splenocytes isolated at day 30 from infected mice were restimulated with gp-33 peptide pulsing and stained for CD107a (A and B), IFN-γ and TNF-α (C and D). Graphs (A, C) illustrate frequencies of CD107a$^+$ (A), IFN-γ$^+$, and TNFα$^+$ among IFN-γ$^+$ (C) *Ptpn11*-deficient and control P14 T cells, and representative flow cytometry pictures are shown (B, D). Results depict mean ± SEM of n=3-4 (Armstrong) and n=5-6 (clone 13) (A and C). Results confirm data shown in Figure 4B and C and were performed once with gp-33 restimulation (A and B) or are representative of at least two independent experiments (C and D). E and F) Viral titers at the indicated times in serum (E) and 34 days after infection with LCMV clone 13 in the kidney (F) from *CD4cre Ptpn11*$^{wt/wt}$, *CD4cre Ptpn11*$^{fl/fl}$ and *Ptpn11*$^{fl/fl}$ mice. Results illustrate mean ± SEM of n=4-9 mice/group (E) and n=6-12 mice/group (F) and are a pool of two independent experiments. Only statistically significant differences are shown; *p ≤ 0.05, Student's t-test.

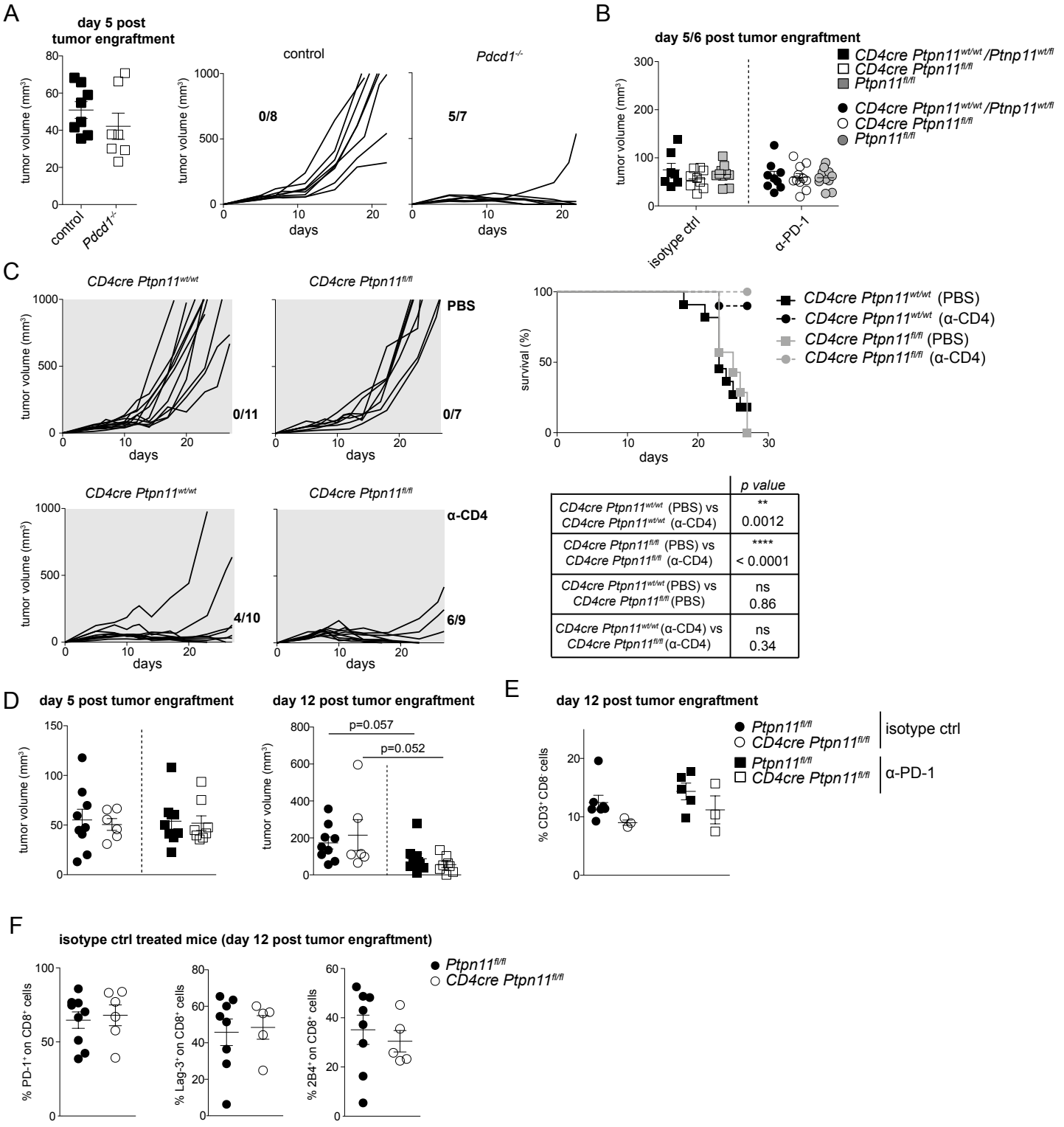

Figure S5. Control of MC38 engraftment in the absence of PD-1 signaling, helper T cells, and Shp2. Related to Figure 5.
A) Wild type and *Pdcd1*-deficient mice were subcutaneously inoculated with MC38 cells. Tumor growth in individual mice is shown at day 5 (*on the left*) and over time (*on the right*); the number of mice completely controlling tumor growth in each group is indicated within the graphs. B) Mice of the indicated genotypes were subcutaneously inoculated with MC38 cells. Graph depicts tumor volume 5-6 days after (depending on the experiment), when mice were randomized as indicated and treatment with α-PD1 antibody or isotype control was started. C) *CD4cre Ptpn11$^{wt/wt}$* and *CD4cre Ptpn11$^{fl/fl}$* mice were depleted of CD4$^+$ T cells by weekly i.p. injections of α-CD4-depleting antibody (GK1.5, BioXcell, 200 µg/mouse), or PBS as control, starting two days prior to MC38 engraftment. Tumor growth in individual mice is shown (*on the left*); the number of mice completely controlling tumor growth in each group is indicated next to the graphs. Survival curves and statistical comparisons are shown (*on the right*). D-F) *CD4cre Ptpn11$^{fl/fl}$* and *Ptpn11$^{fl/fl}$* mice were inoculated with MC38 cells. D) Graphs show tumor volume 5 days after inoculation (*on the left*), when mice were divided as indicated and treatment with α-PD-1 antibody or isotype control was started, and 12 days (*on the right*) after inoculation and three injections of α-PD1 antibody or isotype control. E) Graph depicts the percentage of infiltrating T helper cells (gated as CD8$^-$ CD3$^+$, which largely correspond to CD4$^+$ T lymphocytes) in isotype and α-PD-1 antibody-treated mice among hematopoietic cells. F) Percentage of PD-1$^+$, Lag-3$^+$, and 2B4$^+$ among CD8$^+$ T cells infiltrating tumors from isotype-treated *CD4cre Ptpn11$^{fl/fl}$* and *Ptpn11$^{fl/fl}$* mice. Results depict n=7-11 mice/group (C, *right panel*), and mean ± SEM of n=7-8 mice/group (A, *left panel*), of n=9-11 mice/group (B), of n=3-9 mice/group (D-F). Data are a pool of two independent experiments (A-D and F) and a representative graph of two independent experiments (E). Only statistically significant differences are indicated; Student's t-test. C) For survival, comparisons are by log-rank (Mantel-Cox) test.

Supplemental Experimental procedures

Flow cytometry: surface and intracellular staining
For flow cytometry analysis, cells were pre-incubated with α-CD16/32 (2.4G2) to block Fc receptors and then surface stained using antibodies against CD3e (145-2C11), CD4 (GK1.5, RM4-5), CD5 (53-7.3), CD8a (53-6.7), CD24 (M1/69), CD44 (IM7), CD45.1 (A20), CD45.2 (104), CD62L (MEL-14), CD69 (H1.2F3), PD-1 (J43, 29F.1A12), Lag3 (ebioC9B7W), 2B4 (ebio244F4), Tigit (1G9), and CD107 (ebio1D4B). Antibodies were purchased from eBioscience or Biolegend. The H-2Db–gp33 H-2Db–gp276 tetramer was from TCMetrix. Stainings were performed with appropriate combinations of fluorophores; streptavidin conjugated fluorophores were from eBioscience. To gate on thymocytes, the lineage mix used contained anti-B220 (RA3-6B2), -NK1.1 (PK136), -F4/80 (BM8), -CD11c (N418), and -TCRγδ (eBioGL3). Proliferation was assessed by the detection of Ki67 ex vivo. Intracellular staining for Ki67 (anti-Ki67, clone SolA15) was performed post surface staining using the Transcription factor fixation/permeabilization buffer from eBioscience following the recommended protocol. Transcription factors were detected using the transcription factor staining kit from eBioscience and staining with mAbs for Eomes (Dan11mag), T-bet (eBio4B10) (both from eBioscience) or Tcf1 (C63D8, Cell Signaling) followed by anti-rabbit IgG APC (SouthernBiotech). Data were acquired with a Becton Dickinson flow cytometer and analysed using FlowJo software (Tree Star).

Cytokine production/degranulation capacity assay
Total splenocytes from LCMV-infected mice were cultured for two hours with anti-CD3 or anti-CD3/CD28 (coated overnight with 2 μg/ml anti-CD3e (145-2C11-ebio, eBioscience) only, or 2 μg/ml anti-CD3e and 2 μg/ml of anti-CD28 (37.51, eBioscience)). Then, Brefeldin A (10 μg/ml) was added and cells were cultured for two additional hours. For gp33 peptide restimulation, total splenocytes were incubated 4 hours with 1 μM LCMV gp (33-41) peptide (EMC microcollections), in the presence of Brefeldin A (10 μg/ml) for the last 3 hours. Cells were first surface stained, then fixed with 4% paraformadeyde and permeabilized with 0.5% saponin (Sigma) in PBS for 15 minutes. After permeabilization, cells were then stained for the indicated cytokines (TNF-α clone MP6-XT22, IFN-γ clone XMG1.2, IL-2 clone JE6-5H4). Degranulation capacity was determined incubating the cells during the stimulation with anti-CD107 (ebio1D4B).

Immunoblot analysis
Total T cells and $CD8^+$ T cells were enriched using α-CD4 and α-CD8a magnetic beads or α-CD8a magnetic beads (Miltenyi Biotec) only, respectively. T cell purity was over 90%, whereas T cell contamination in T cell-depleted spenocytes less than 5%. Rabbit polyclonal anti-mouse Shp-2 (D50F2) and Shp-1 (C14H6) were obtained from Cell Signaling. α-β-actin was from Abcam.

Quantitative PCR
RNA extraction, retrotranscription to cDNA, and expression analysis were done as previously described (Ludigs et al., 2015). The Following primers were used:

Ptpn11 fwd: 5'- AGACTTCGTTCTCTCCGTGC-3'
Ptpn11 rev 5'- CTGTCAGAGAGTCAAAGCGC-3'

polr2a fwd 5'- CCGGATGAATTGAAGCGGATGT-3'
polr2a rev: 5'-CCTGCCGTGGATCCATTAGTCC-3'

Supplemental References
Grossmann, K.S., Wende, H., Paul, F.E., Cheret, C., Garratt, A.N., Zurborg, S., Feinberg, K., Besser, D., Schulz, H., Peles, E., et al. (2009). The tyrosine phosphatase Shp2 (PTPN11) directs Neuregulin-1/ErbB signaling throughout Schwann cell development. Proceedings of the National Academy of Sciences of the United States of America 106, 16704-16709.
Ludigs, K., Seguin-Estevez, Q., Lemeille, S., Ferrero, I., Rota, G., Chelbi, S., Mattmann, C., MacDonald, H.R., Reith, W., and Guarda, G. (2015). NLRC5 Exclusively Transactivates MHC Class I and Related Genes through a Distinctive SXY Module. PLoS genetics 11, e1005088.
Nishimura, H., Minato, N., Nakano, T., and Honjo, T. (1998). Immunological studies on PD-1 deficient mice: implication of PD-1 as a negative regulator for B cell responses. International immunology 10, 1563-1572.
Pircher, H., Moskophidis, D., Rohrer, U., Burki, K., Hengartner, H., and Zinkernagel, R.M. (1990). Viral escape by selection of cytotoxic T cell-resistant virus variants in vivo. Nature 346, 629-633.